Supporting information for:

Homo-endotaxial one-dimensional Si nanostructures

Jiaming Song[1], Bethany M. Hudak[1], Hunter Sims[1,2], Yogesh Sharma[1], T. Zac Ward[1], Sokrates T. Pantelides[1,2], Andrew R. Lupini[1], Paul C. Snijders[1,3*]

1. Materials Science and Technology Division, Oak Ridge National Laboratory, Oak Ridge, Tennessee 37831, USA
2. Department of Physics and Astronomy, Vanderbilt University, Nashville, Tennessee 37235, USA
3. Department of Physics and Astronomy, The University of Tennessee, Knoxville, Tennessee 37996, USA

* Corresponding Author: Paul C. Snijders; Email: snijderspc@ornl.gov

Supplementary Note 1

Si capping layers were grown on the Bi nanoline template surface. Fig. S1a presents a high-resolution Z-contrast cross-sectional STEM images of Bi nanoline surfaces capped at 400 °C in the presence of a Bi surfactant layer [1–3] showing that this results in a homoepitaxial crystalline capping layer. The original substrate location was determined in two ways. First we used a constant Si deposition rate during growth. Using a partial mask and by evaluating the film thickness after growth using scanning probe microscopy, we extracted the growth rate of the Si capping layer. This growth rate was cross-checked with STEM by extracting the capping layer thickness using the easily identified interface in samples where the Haiku cores survive capping layer growth. When the capping layer was grown at 400 C in the presence of a Bi surfactant layer, no Si Haiku cores can be found, and the Bi atoms have mostly disappeared, consistent with their low solubility in Si [4,5]. (An STM surface characterization of the surfactant-covered nanoline template surface is presented in Supplementary Note 2.)

We have also capped the Bi nanolines in the presence of a Bi surfactant layer at an intermediate growth temperature of 250 °C, where very thin c-Si layers can be grown [6]. STEM imaging shows that the reconstructed Si nanoline cores survive at this temperature (Fig. S1b). Moreover, at this temperature the first few layers of the capping layer grow with a somewhat crystalline structure, especially in between the nanolines. On top of the nanolines, however, the structure is more disordered and no clear evidence of the two rows of Bi atoms from the Bi nanolines can be detected. The remainder of the amorphous capping layer appears devoid of Bi, indicating that the low Bi solubility in Si drives significant Bi surface segregation already during growth at 250 °C.

On the other hand, upon capping with Si at room temperature, the Haiku cores do survive with a locally larger concentration of Bi atoms spread in the capping layer near the surviving cores, as discussed in the main text (Fig. 2a), suggesting that the diffusion of Bi can be limited by decreasing the temperature during capping layer growth. Decreasing the capping layer growth temperature, and thus the Bi mobility, even more to -90 °C indeed results in an additional decrease in the concentration of Bi in the capping layer, and a complementarily increased Bi concentration in the direct vicinity of the still-present reconstructed Si cores, see Fig. S1c.

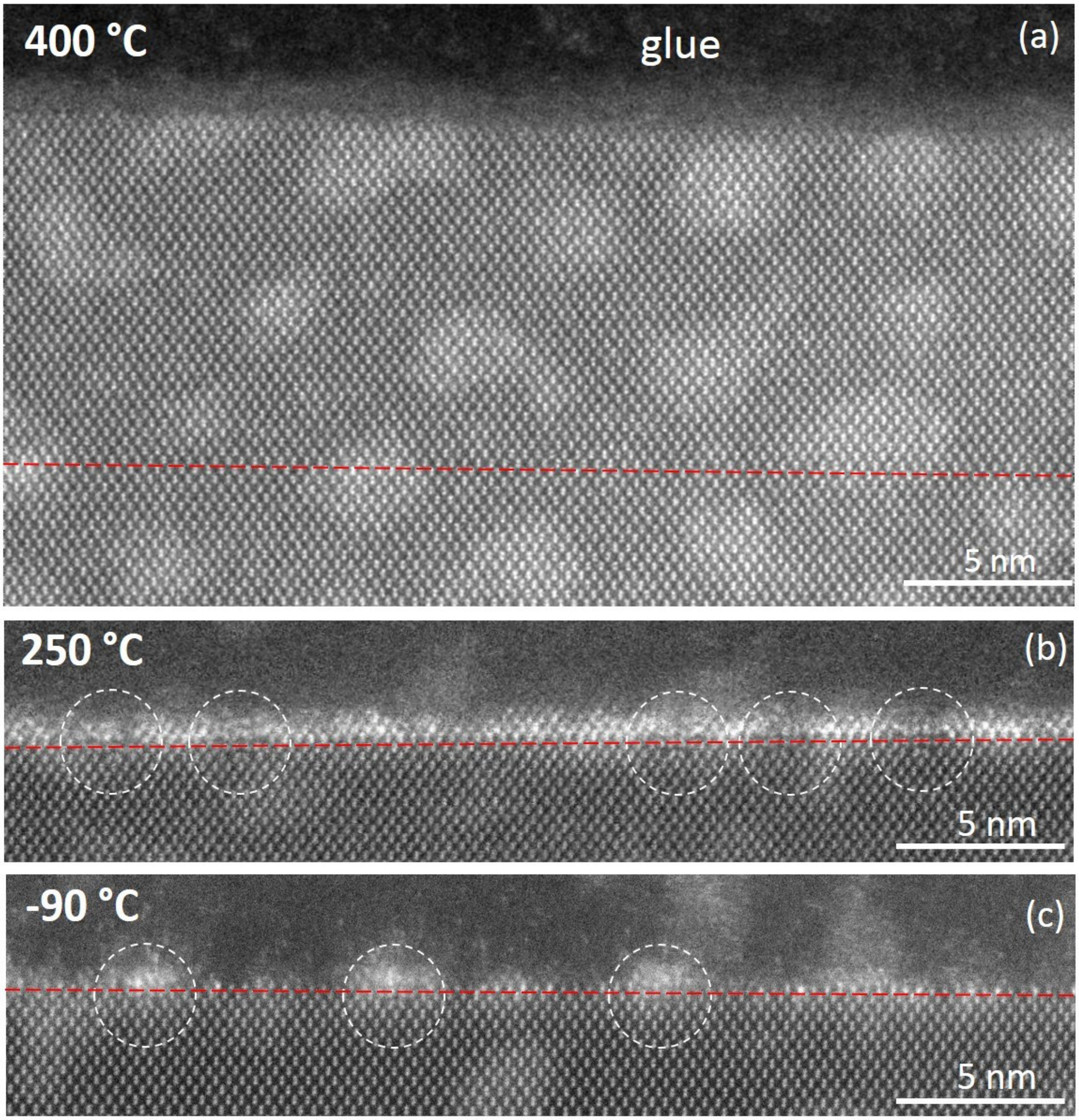

Fig. S1 Cross-sectional STEM images for Si(100) substrates that were covered by Bi-induced nanolines and were imaged after deposition of (a) an approximately 1 ML Bi surfactant layer and a ~10 nm capping layer with Si at 400 °C, (b) 250 °C, and (c) a-Si without a Bi surfactant layer at low temperature. The red dashed lines indicate the position of the surface of the original Si(100) substrate before capping as inferred from the reconstructed Si cores. White dashed circles mark reconstructed core structures.

Supplementary Note 2

In order to ascertain whether the Bi nanolines remain intact after depositing a Bi surfactant layer, we imaged the resulting surface with STM. Fig. S2a and b show a Si(100) surface containing Bi nanolines after deposition of a Bi surfactant layer of approximately one ML at room temperature. Casual inspection reveals that at this temperature, the ordered (2×n) superstructure that is present on the Si(100) due to vacancy ordering does not form upon room temperature Bi deposition [2], consistent with the LEED pattern (inset in Fig. S2a) that shows dimmer (2×1) spots as compared to the LEED pattern in Fig. 1a. It is also immediately obvious that the Bi nanolines appear as trenches instead of higher stripes as observed on the clean Si(100) surface, Fig. 1a. Fig. S2b shows a higher resolution image of the same surface as Fig. S2a, and in Fig. S2c, a line profile taken across a Bi nanoline (see Fig. S2b) is presented. The distance between two the two Bi lines visible on this nanoline is 6.3 Å, consistent with that of nanolines on a surface without surfactant layer, see Figs. 1b and d. Clearly, the Bi surfactant layer mostly covers the (2×1) dimer structure on the bare Si(100) surface and leaves the Bi nanolines intact [7,8]. We surmise that this happens due to the energy gain by the passivation by Bi of the dangling bond on each Si atom of the dimers on the (2×1) Si(100) surface; the Bi nanolines do not exhibit partially filled dangling bonds and hence a potential energy gain by additional Bi atoms will be small.

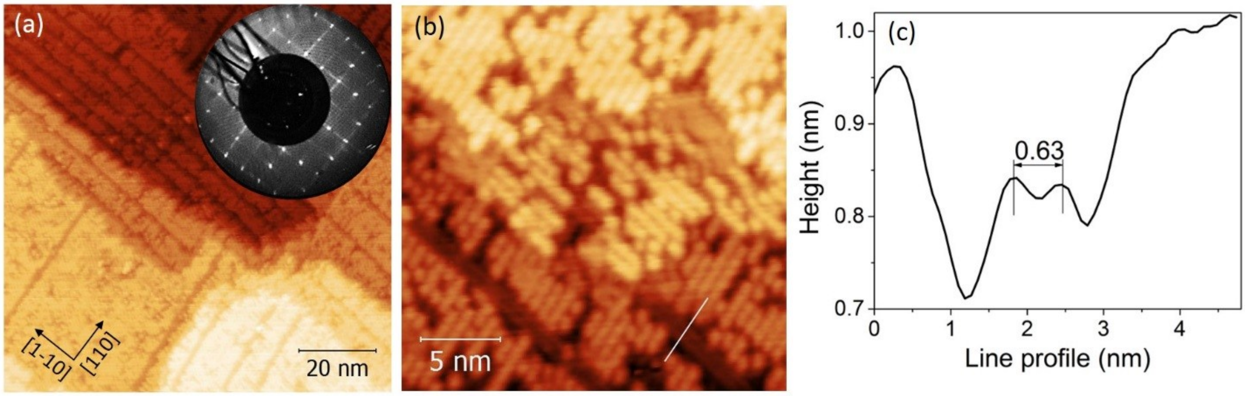

Fig. S2 (a) Large-scale and (b) high-resolution STM topography images of the Bi surfactant layer on a template of Bi nanolines on Si(100). The inset in (a) is a LEED pattern taken at 100 eV. STM scanning parameters: -2.5 V, 400 pA. (c) Line profile recorded as indicated in (b).

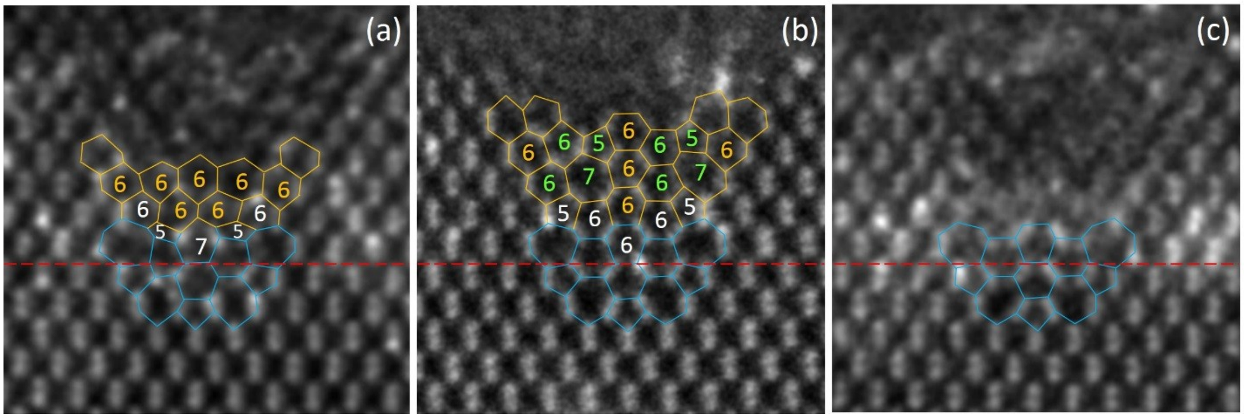

Fig. S3 High-resolution cross-sectional STEM images of a sample with Bi nanolines after capping by the two-step SPE method (see main text). The red dashed lines indicate the surface of the original Si(100) substrate with Bi nanolines before capping.

Supplementary Note 3

We compare the total energies of the normal and modified Haiku structures, as well as the Bi terminated 2×1 surface reconstruction on Si(100), see Fig. S4, in order to confirm that the normal Haiku core has the lowest total energy, and therefore is indeed likely to be the subsurface Si structure that is present at the start of the capping layer growth as our STM results suggest.

Due the difference in the number of Si atoms in the three structures (the normal and modified Haiku cores contain four and two Si atoms less than the Si diamond lattice, respectively), we must take the chemical potential of Si, μ_{Si}, into account by including a term $\Delta N_{Si}\ \mu_{Si}$ in our calculation of the total energies. Here the Si chemical potential is taken as the total energy (per atom) of bulk Si. Our results indicate that the structure with the normal Haiku core is more stable than the modified Haiku and the defect-free Bi structures by 633 meV/Bi dimer (0.21 meV/Å^3) and 528 meV/Bi dimer (0.17 meV/ Å^3), respectively. The significant energy difference between the normal Haiku core structure and the other structures confirms that the modified Haiku core structure is not likely to be present at the start of the capping layer growth, but that the normal Haiku core as identified in the literature [9] is indeed the lowest energy state. This implies that the modified Haiku core forms during capping layer growth. Indeed, the severely distorted Si structure in Fig. S5, formed after placing a single layer of Si atoms above the normal Bi-terminated Haiku structure and allowing the atomic positions to relax, already appears to tend towards a 7-membered ring structure (on the left-hand side of the core structure) reminiscent of those that we observe experimentally in STEM images of the modified Haiku structure.

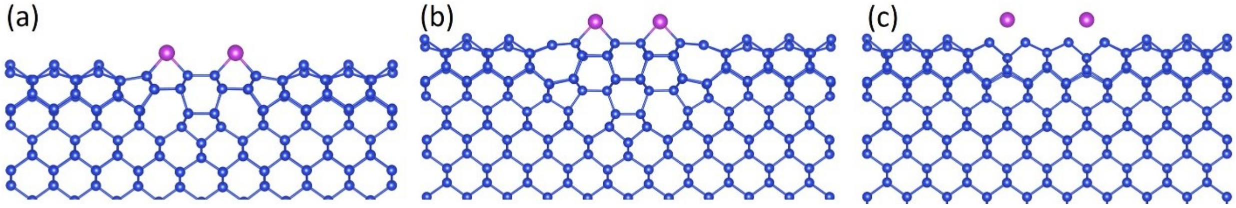

Fig. S4 (a) Normal and (b) modified Haiku structures, and (c) the Bi-terminated Si(100)-2×1 surface.

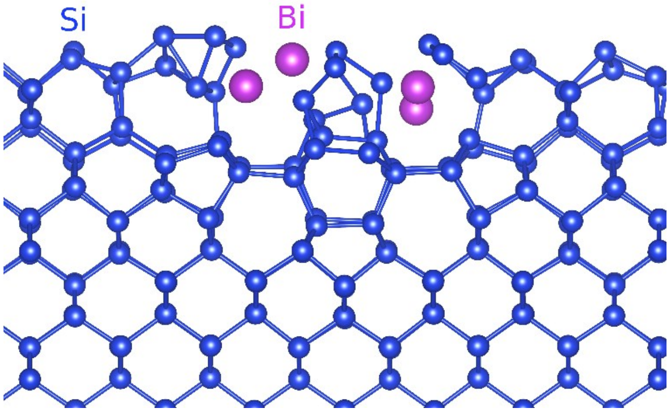

Fig. S5 Structure after adding a monolayer of Si to the Bi-terminated normal Haiku core structure, and relaxing the structure within DFT at 0 K.

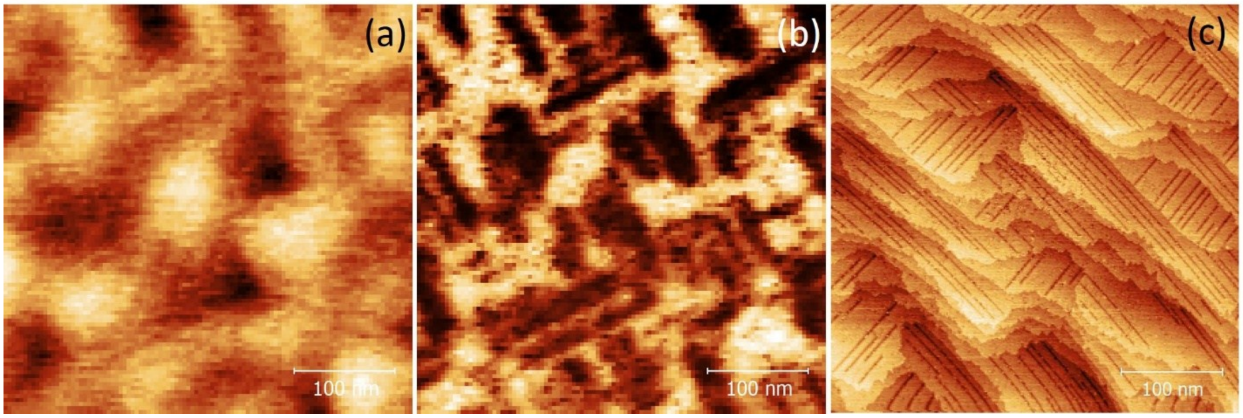

Fig. S6 (a) AFM topography recorded in the same general area as the C-AFM current map (b) cropped from Fig. 4a. (c) STM topography image for the Bi nanoline template with the same lateral scale as (a) and (b). Note that the Bi nanoline density in the STM image is higher than the C-AFM current map due to fluctuations in the local nanoline density.

Supplementary Note 4

STEM sample preparation

Cross-section STEM sample preparation consisted of taking the as-grown sample, cutting it in half, and gluing the halves together to produce a sandwich, which is then sliced into thin sections that are each glued to a support grid. The samples are mechanically polished to approximately 10 microns, and then ion-milled to electron transparency. Immediately before imaging, the samples were baked at a nominal 140 ˚C in vacuum overnight to reduce surface contamination.

STEM imaging details

Atomic-resolution Z-contrast STEM imaging was performed in a Nion UltraSTEM 200 and in a Nion UltraSTEM 100, at accelerating voltages chosen to provide either higher-resolution (200 kV) or reduced sample damage (60 and 100 kV). Convergence angles were nominally 30 mrad, with annular dark field detector (ADF) inner angles of about 80 mrad. Typical probe currents were 30-100 pA with per-pixel dwell times ranging from 4-16 µS. Under these conditions, the expected resolution is between about 0.06 nm (at 200 kV) to 0.1 nm (at 60 kV). The thickness for typical images was measured by EELS as about 0.1-0.2 mean free paths (about 10-20 nm), although both thicker and thinner regions were examined. Images taken far away from the film and glue indicate that the amorphous surface oxide layer was usually about 1 nm thick. In the Z-contrast mode, the intensity depends on the sample thickness (number of atoms) and approximately the square of the atomic number. The large atomic number (Z=83) means that even single Bi atoms are visible by Z-contrast STEM both on and inside the Si sample (Z=14) for thin samples. For comparison, detection of single dopant atoms in Si [10] and in AlN [11] have previously been reported.

REFERENCES

1 K. Miki, H. Matsuhata, K. Sakamoto, G. a. D. Briggs, J. H. G. Owen and D. R. Bowler, in *Inst. Phys. Conf. Ser.*, IOP Ltd, 1999, p. 167.

2 H. Matsuhata, K. Sakamoto and K. Miki, *J. Electron Microsc. (Tokyo)*, 2004, **53**, 325–337.

3 O. Sakata, W. Yashiro, D. R. Bowler, A. Kitano, K. Sakamoto and K. Miki, *Phys. Rev. B*, 2005, **72**, 121407.

4 K. Murata, P. L. Neumann, T. Koyano, Y. Yasutake, K. Nittoh, K. Sakamoto, S. Fukatsu and K. Miki, *Jpn. J. Appl. Phys.*, 2012, **51**, 11PE05.

5 K. Murata, Y. Yasutake, K. Nittoh, K. Sakamoto, S. Fukatsu and K. Miki, *Appl. Phys. Express*, 2010, **3**, 061302.

6 L. Oberbeck, N. J. Curson, T. Hallam, M. Y. Simmons, G. Bilger and R. G. Clark, *Appl. Phys. Lett.*, 2004, **85**, 1359–1361.

7 C. Park, R. Z. Bakhtizin, T. Hashizume and T. Sakurai, *Jpn. J. Appl. Phys.*, 1993, **32**, L528–L531.

8 J. H. G. Owen, F. Bianco, S. A. Köster, D. Mazur, D. R. Bowler and C. Renner, *Appl. Phys. Lett.*, 2010, **97**, 093102.

9 J. H. G. Owen, K. Miki, H. Koh, H. W. Yeom and D. R. Bowler, *Phys. Rev. Lett.*, 2002, **88**, 226104.

10 P. M. Voyles, D. A. Muller, J. L. Grazul, P. H. Citrin and H.-J. L. Gossmann, *Nature*, 2002, **416**, 826–829.

11 R. Ishikawa, R. Mishra, A. R. Lupini, S. D. Findlay, T. Taniguchi, S. T. Pantelides and S. J. Pennycook, *Phys. Rev. Lett.*, 2014, **113**, 155501.